Spontaneous electrochemical uranium extraction from wastewater with net electrical energy production

Yin Ye
Northwestern Polytechnical University https://orcid.org/0000-0003-2507-2767
Jian Jin
Northwestern Polytechnical University
Wei Han
Northwestern Polytechnical University
Shiyu Miao
Qinghai University
Yanyue Feng
Chalmers University of Technology
Zemin Qin
Northwestern Polytechnical University
Xin Tang
Northwestern Polytechnical University
Cui Li
Northwestern Polytechnical University
Yanlong Chen
Northwestern Polytechnical University
Fan Chen (chenfanhit@gmail.com)
https://orcid.org/0000-0001-9357-0827
Yuheng Wang
Northwestern Polytechnical University

Article

Keywords:

Posted Date: June 8th, 2022

DOI: https://doi.org/10.21203/rs.3.rs-1715307/v1

Spontaneous electrochemical uranium extraction from wastewater with net electrical energy production

Yin Ye [1], Jian Jin [1], Wei Han [1], Shiyu Miao [2], Yanyue Feng [3], Zemin Qin [1], Xin Tang [1], Cui Li [1], Yanlong Chen [1], Fan Chen [1*], Yuheng Wang [1*]

[1] *School of Ecology and Environment, Northwestern Polytechnical University, 710129 Xi'an, P. R. China*

[2] *College of Eco-Environmental Engineering, Qinghai University, Xining, 810016, P. R. China*

[3] *Department of Chemistry and Chemical Engineering, Chalmers University of Technology, SE-41296 Gothenburg, Sweden*

[*] Corresponding authors:

Fan Chen: fan.chen@nwpu.edu.cn

Yuheng Wang: yuheng.wang@nwpu.edu.cn

Abstract

Extracting uranium from uranium-mine wastewater is highly important from both the environmental protection and the resource preservation perspectives. However, conventional adsorption methods and zero-valent-iron induced reductive precipitation methods have intrinsic limitations. Here we demonstrate a spontaneous electrochemical (SPEC) method that spatially decouples the uranium-adsorption-reduction reactions and the iron oxidation reaction, enabling stable and efficient uranium extraction with net electrical energy output. U(VI) species are firstly adsorbed on a carbonaceous electrode, and subsequently reduced by electrons derived from iron oxidation. In simulated wastewater, the SPEC method achieves a 12 times higher uranium extraction efficiency without saturation of the carbonaceous electrode, in comparison with the adsorption method. In real wastewater, the uranium extraction efficiency reaches 352 $mg \cdot g^{-1}$ during 60 h operation with simultaneous net electrical energy production (0.65 $Wh \cdot m^{-2}$), and the operation cost is only 3.46~5.99 $USD \cdot kgU^{-1}$. This work potentially opens a new avenue for cost-effective uranium recovery from mine wastewater.

As a reliable low-carbon energy source, nuclear power has avoided ~74 Gt of CO_2 emissions over the past 50 years, hence playing a crucial role in attaining carbon neutrality [1]. The nuclear power production is predicted to increase in the near future [2]. However, concerns about its sustainability have arisen. First, the security of nuclear fuel supply is questioned. Uranium, a vital nuclear fuel, is mainly supplied from terrestrial mines, but recent predictions have warned that the terrestrial uranium reserves could be depleted within a century at the current consumption rate [3, 4, 5]. Another concern is the environmental impact of uranium mining activities. Mining and milling of uranium ores generate large quantities of wastewater containing highly mobile and toxic hexavalent uranium, *i.e.* U(VI) (present as UO_2^{2+}, or its complexes). If not properly treated, these uranium-bearing wastewaters will contaminate the adjacent environment and threaten the local eco-system [6, 7]. Extracting uranium from mine wastewater is therefore highly interesting, because it simultaneously reduces the negative environmental footprint of the nuclear power industry and alleviates the depletion of conventional uranium resources.

One possible avenue is the physicochemical adsorption methods [8, 9, 10, 11, 12]. The uranium extraction capacity of a physicochemical adsorption process is constrained by the number of active sites available and accessible to U(VI) species. The availability of active adsorption sites would decrease as the adsorption proceeds, and the adsorbed U(VI) species would repulse other incoming U(VI) species due to Coulomb repulsion, lowering the overall accessibility of available active sites [3]. Once all accessible active sites are saturated, the adsorption of U(VI) stops. This is an intrinsic limitation of physicochemical adsorption methods. Recent studies have shown that the application of a direct current can reduce the surface-adsorbed U(VI) species and avoid Coulomb repulsion, and therefore significantly promote uranium extraction [3, 13, 14, 15], but these methods are rather energy-consuming. Meanwhile, as uranium in its tetravalent state, *i.e.* U(IV), is sparingly soluble and much less toxic, reducing U(VI) to U(IV) is another viable approach for uranium extraction. Among different reductants, zero-valent-iron (ZVI) has attracted tremendous research interests, because of its inexpensive and easily accessible nature, and the Fe/Fe^{2+} redox couple has high reactivity and reduction power to drive

U(VI)-to-U(IV) reduction [7, 16, 17]. During ZVI-driven uranium extraction, soluble U(VI) species are firstly adsorbed onto the surface of ZVI, and subsequently reduced to U(IV) deposits [7, 18]. Nanoscale ZVI materials (nZVI) are therefore favorable because of their large specific surface area [19, 20, 21, 22]. However, as the extracted U(IV) products co-precipitate with nZVI, costly separation processes for their recovery are required. In addition, nZVI is prone to oxidation in air and surface passivation in aqueous solutions, and tend to form aggregation in complex water matrices, leading to significant reactivity loss of nZVI over operation time [23, 24, 25]. If the Fe-to-Fe^{2+} oxidation and the U(VI)-to-U(IV) reduction can be spatially decoupled, the use of nZVI and the associated drawbacks can be eliminated. The electrons derived from ZVI can be utilized to reduce the surface-adsorbed U(VI) to sparingly soluble U(IV), further promoting the uranium extraction capacity of a sorbent.

Inspired by these analyses, here we present a spontaneous electrochemical (SPEC) method driven by ZVI oxidation for uranium extraction with simultaneous energy recovery. In the SPEC system, the U(VI) adsorption occurs on the surface of a porous carbonaceous cathode, while the Fe^0-to-Fe^{2+} oxidation takes place in the anodic chamber providing electrons flow through an extern circuit to the cathode to drive the U(VI)-to-U(IV) reduction. The SPEC method has achieved a uranium extraction capacity of 2438 $mg \cdot g^{-1}$ in simulated wastewater and 352 $mg \cdot g^{-1}$ in real uranium-mine wastewater without saturation, and the uranium extraction products are easily recoverable. The whole uranium extraction-recovery process requires no energy input, and net electrical energy production has been attained. This study potentially provides a new avenue for the development of energy- and cost-efficient uranium extraction technology.

Main text

Theoretical feasibility of the SPEC method

The concept of the proposed SPEC method for uranium extraction is illustrated in Figure 1a. During operation, the anodic reaction is the Fe^0-to-Fe^{2+} oxidation (Equation 1) because it is more thermodynamically favorable than the Fe^0-to-Fe^{3+} oxidation [26], while the desired cathodic reaction is the U(VI)-to-U(IV) reduction (Equation 2). At standard conditions, the SPEC system

can theoretically generate an open-cell voltage (OCV) of 0.767 V (overall reaction shown in Equation 3) as a driving force for the electron flow that allows simultaneous electrical energy recovery.

$$U(VI) + 2e^- \rightarrow U(IV) \quad E^0 = +0.327\ V\ vs.SHE \quad \textbf{Equation 1}$$

$$Fe^{2+} + 2e^- \rightarrow Fe \quad E^0 = -0.440\ V\ vs.SHE \quad \textbf{Equation 2}$$

$$Fe + U(VI) \rightarrow U(IV) + Fe^{2+} \quad E^0 = +0.767\ V\ vs.SHE \quad \textbf{Equation 3}$$

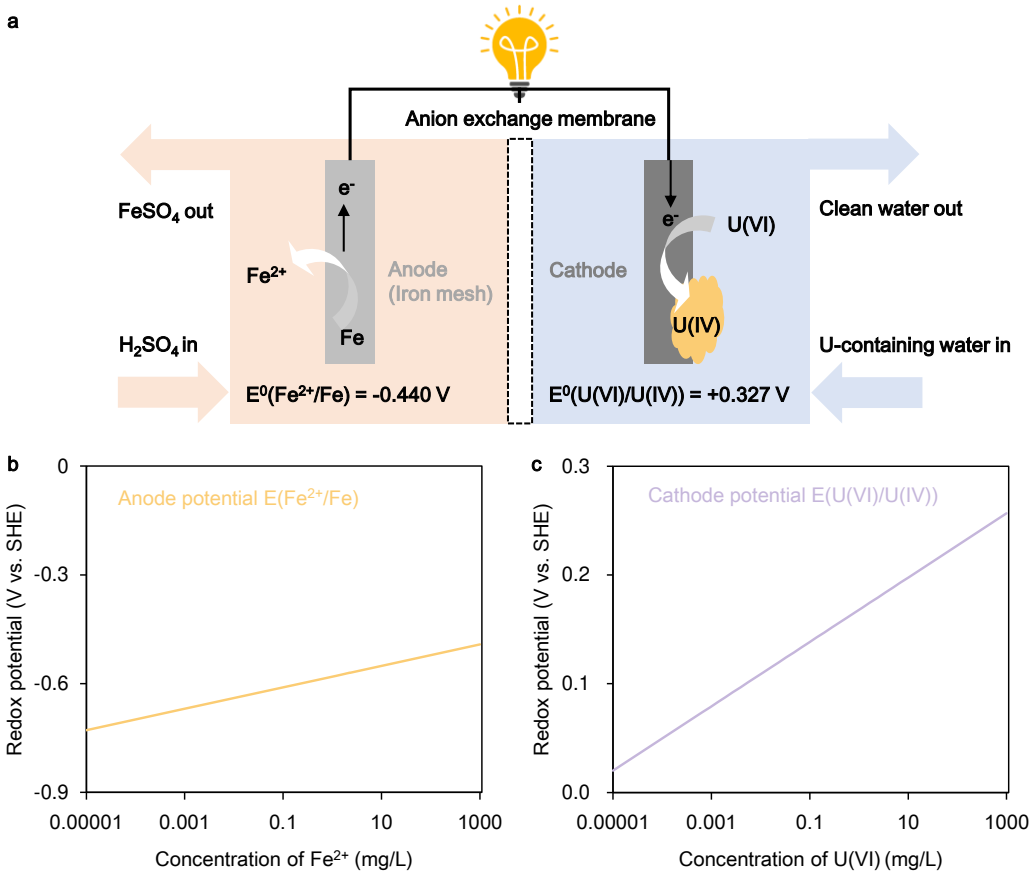

Figure 1. The SPEC method. (a) The schematic representation of the SPEC uranium extraction method; (b) The calculated anode potential as a function of Fe^{2+} concentration; (c) The calculated cathode potential as a function of U(VI) concentration.

The Fe^{2+} concentration and the U(VI) concentration are important factors affecting the OCV, *i.e.* driving force, of the SPEC system, according to the Nernst equation. In practical implementations, the concentration of Fe^{2+} in the anode chamber will increase as the operation proceeds, and the U(VI) concentration can vary significantly among different wastewaters and will decrease as the extraction proceeds. To further assess the theoretical feasibility of the SPEC

method, we used the Nernst equation to model the anode potential, *i.e.* E(Fe^{2+}/Fe), as a function of Fe^{2+} concentration and the cathode potential, *i.e.* E(U(VI)/U(IV)), as a function of U(VI) concentration. The results show that the anode potential increases with increasing Fe^{2+} concentration as the operation proceeds, and the cathode potential decreases with decreasing U(VI) concentration (Figure 1b and c). Nevertheless, even when high Fe^{2+} concentration (1000 $mg \cdot L^{-1}$) and extremely low U(VI) concentration (0.00001 $mg \cdot L^{-1}$) are combined, the SPEC system still has a theoretical OCV of ~0.512 V, representing sufficient driving force. Thus, the proposed SPEC uranium extraction method is feasible from the thermodynamics perspectives.

Proof of principle

Following the theoretical analysis described above, we carried out experiments in uranium-bearing simulated wastewater to evaluate the practical feasibility of the SPEC method. An H-type two-chambered (250 mL: 250 mL) SPEC system consisting of an iron mesh anode and a chitosan-modified carbon felt (CCF, characterizations shown in Supplementary Figure 1) cathode was constructed for the proof-of-principle tests. Diluted H_2SO_4 solution was used as the anolyte, while uranium-bearing simulated wastewater was filled in the cathode chamber. We first assessed the electrical energy recovery capacity of the SPEC system with varied anolyte pH using linear sweep voltammetry (LSV). The obtained polarization curves and the corresponding power curves are shown in Figure 2a and b, and they suggest that the low pH of anolyte would benefit the electrical energy recovery. As the anolyte pH should not affect the redox potential of the Fe^{2+}/Fe couple according to the Nernst equation, it might influenced the energy recovery capacity by changing the conductivity of the anolyte.

We subsequently evaluated the uranium extraction performance of the SPEC method in comparison with physicochemical adsorption, in a series of simulated wastewater with varied initial uranium concentrations ranging from 5 $mg \cdot L^{-1}$ to 100 $mg \cdot L^{-1}$. This concentration range covers most reported uranium concentrations in real mine wastewaters [27, 28, 29, 30, 31]. The physicochemical adsorption method showed a saturation uranium extraction efficiency of ~52 $mg \cdot g^{-1}$, and in contrast the SPEC method exhibited significantly higher uranium extraction efficiency (Supplementary Figure 2). The uranium extraction capacity of the SPEC system

increased drastically with the increasing initial uranium concentration (Figure 2c), and the difference in uranium extraction performance between the two methods became greater at high initial uranium concentrations (Supplementary Figure 2): with an initial concentration of 100 $mg \cdot L^{-1}$, the SPEC method achieved a uranium extraction efficiency of 606 $mg \cdot g^{-1}$ after 23 h operation, which was 12 times higher than that achieved by adsorption at identical conditions. The superior performance of the SPEC method can be explained by the fact that the extracted U(VI) species were constantly reduced by electrons, which would alleviate the Coulomb repulsion between extracted uranium species and aqueous U(VI) [3, 13, 14, 15]. These uranium species extracted by the SPEC method may also act as active sites for further uranium extraction reactions (which will be discussed in detail in the following section). As a result, the saturation uranium extraction capacity of the SPEC method is much larger than the adsorption method, when identical material is applied. To test this hypothesis, we conducted an additional SPEC extraction experiment with an extremely high initial uranium concentration (1000 $mg \cdot L^{-1}$), and the SPEC method showed a high uranium extraction efficiency of 2438 $mg \cdot g^{-1}$ after 46 h operation without showing a saturation trend.

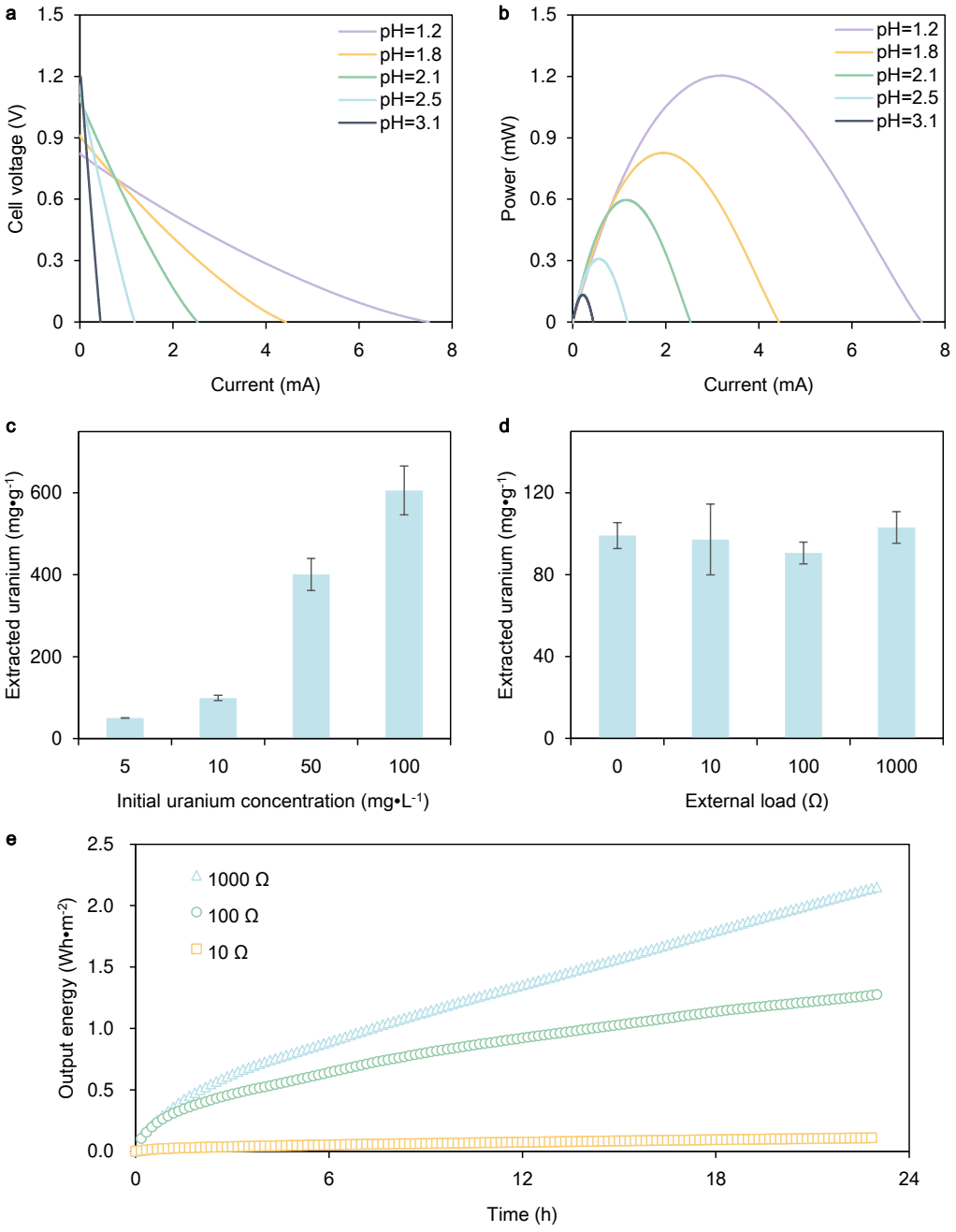

145

146 **Figure 2. Uranium extraction from water by the SPEC method with simultaneous**
147 **energy recovery. (a) Polarization curves of the SPEC sytem containing H_2SO_4 solutions**
148 **at varied pH as the anodic solution and simulated uranium-containing wastewater (10**
149 **mg·L^{-1}) as the cathodic solution; (b) Power of the SPEC system calculated according to**
150 **the polarization curves; (c) Total uranium extraction efficiency of the SPEC method**
151 **after 23 h operation in simulated uranium-containing wastewater with varied initial**
152 **uranium concentration ($[U]_0$); (d) Total uranium extraction efficiency of the SPEC**

mthod after 23 h operation in simulated uranium-containing wastewater ($[U]_0$ = 10 $mg \cdot L^{-1}$) with varied extrernal load; (e) The accumulated output energy density as a function of operation time during SPEC uranium extraction in simulated uranium-containing wastewater ($[U]_0$ = 10 $mg \cdot L^{-1}$) with varied external load. Conditions: effective area of the CCF electrode was 2.5 cm^2.

A series of SPEC uranium extraction experiments were carried out with varied external load (0 ~ 1000 Ω), to evaluate the electrical energy recovery capacity of the SPEC method. The results show that the uranium extraction performance of the SPEC system did not vary noticeably as the external load was increased from 0 Ω to 1000 Ω (Figure 2d), while the output electrical energy from the SPEC system increased with increasing external load (Figure 2e). The results present herein clearly evidenced that the proposed SPEC method can simultaneously achieve uranium extraction and electrical energy recovery.

Analysis of the extracted uranium and the mechanisms of the SPEC method

The extracted uranium species were analyzed to decipher the mechanisms of the SPEC uranium extraction method. First, the morphologies of the extracted uranium species after 23 h of extraction by both the SPEC method and the adsorption method were characterized and compared. A thick pale yellow layer was directly visualized on the CCF electrode after SPEC extraction, but no noticeable morphological change of the CCF electrode was seen in the case of adsorption (Figure 3a). SEM images confirmed the formation of micrometer-sized particles in the case of SPEC extraction, while the surface of the CCF electrode remained smooth without the formation of any precipitates in the case of adsorption (Figure 3b and Supplementary Figure 4). SEM images with higher magnification show that the micrometer-sized particles observed in the case of SPEC extraction have similar cuboid-like morphologies, and the EDS results suggest they mainly consisted of U and O (Figure 3c and d). These results reveal that uranium extraction proceeded via a phase-transforming pathway during the SPEC extraction.

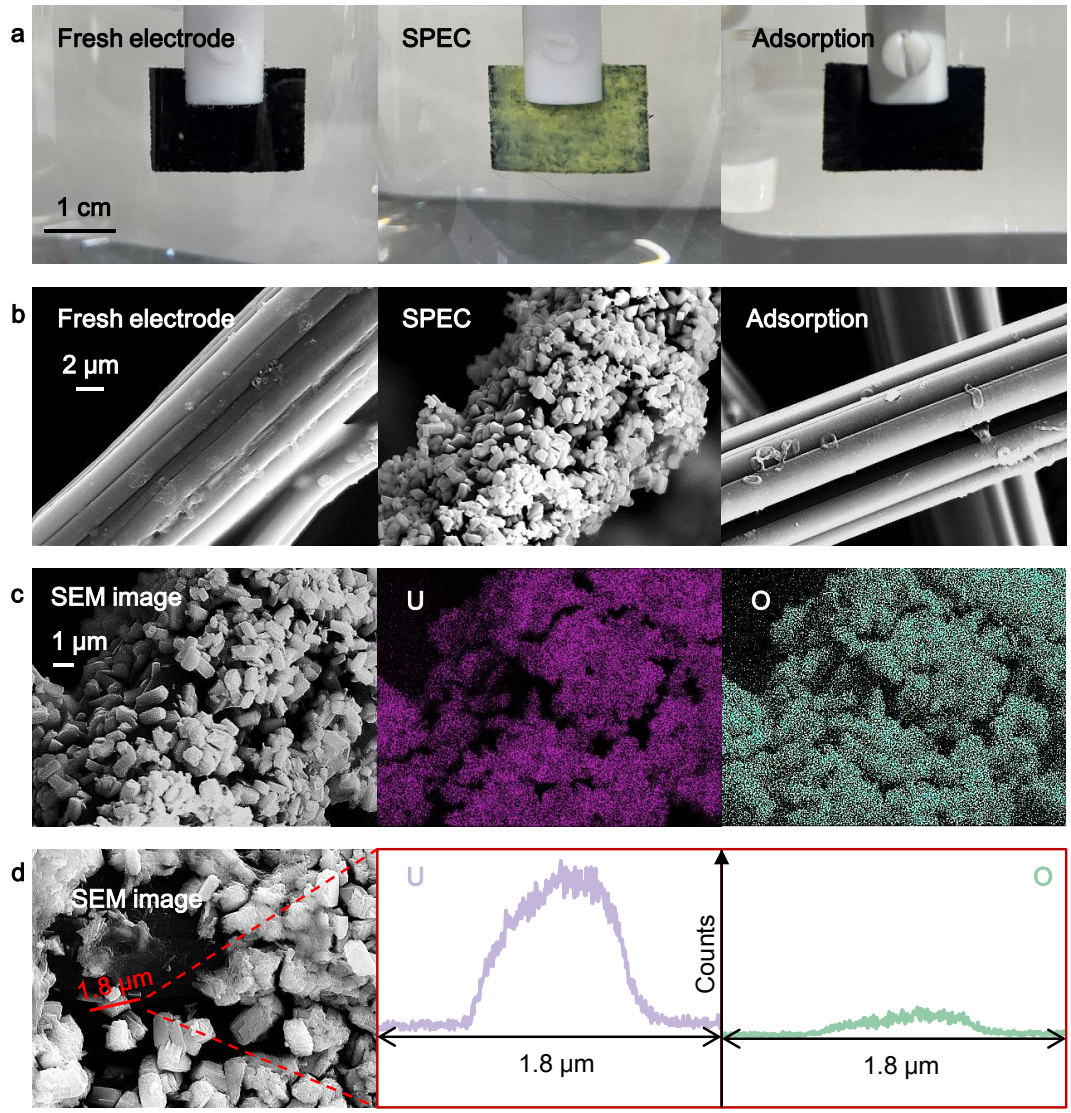

Figure 3. Morphological characterizations of the extracted uranium. (a) Photographs of the fresh CCF electrode, the CCF electrode after 23 h of uranium extraction via the SPEC method, and the CCF electrode after 23 h of uranium extraction via the adsorption method; (b) SEM images of the fresh CCF electrode, and the CCF electrode after 23 h of uranium extraction using the SPEC method and the adsorption method; (c) EDS mapping showing the elemental composition and distribution of the surface deposition layer of the CCF electrode after SPEC uranium extraction; (d) EDS line scan of a microparticle in the surface deposition layer shown in (c). Conditions: Simulated wastewater with $[U]_0$ = 100 mg·L^{-1}, unadjusted pH, without external load, effective area of CCF electrode was 2.5 cm^2.

The valence state of the uranium precipitates formed after SPEC extraction was studied through XPS U4f analysis. The spectrum shows two major peaks separated from each other by ~10.8 eV, and a small peak on the higher binding energy side (Figure 4a). The two major peaks located at ~380.0 eV and ~390.8 eV could be assigned to the primary peaks of $U4f_{7/2}$ and $U4f_{5/2}$, respectively, and the small peak at ~397.4 eV is the satellite peak of $U4f_{5/2}$. The peak separation of 6.8 eV between the satellite peak and the $U4f_{5/2}$ primary peak suggests the presence of U(IV) in SPEC extracted uranium [32, 33, 34], and the fitting results reveal the dominance of U(IV) content; in contrast, uranium species extracted by adsorption mainly consisted of U(VI) (Supplementary Figure 5). Through XRD characterization, the uranium precipitates obtained from SPEC extraction were identified as $(UO_2)O_2 \cdot 2H_2O$, a U(VI) peroxide crystal also known as metastudtite (Figure 4b). The structure of these metastudtite species was also confirmed by EXAFS analysis (Figure 4c and d, Supplementary Table 1). The lack of U(IV)-containing phases in the XRD spectrum reveals that the obtained U(IV) species were in amorphous forms. Considering that H_2O_2 could be generated from the reduction of DO by the negatively charged CCF electrode during SPEC extraction [3, 13]. The formation of $(UO_2)O_2 \cdot 2H_2O$ was possibly due to the oxidation of UO_2 by H_2O_2 or $\cdot O_2^-$ species [3, 35, 36], or a result of the reaction of UO^{2+} with H_2O_2 [37]. It is worth mentioning that, although the presence of DO was often deemed detrimental in electrochemical uranium extraction processes [32], we found the beneficial role of DO in the SPEC system studied herein. We compared the uranium extraction performances of the SPEC system in ambient air atmosphere and N_2 atmosphere. The results show that the uranium extraction performance of the SPEC system decreased remarkably when operating in N_2 atmosphere (Supplementary Figure 6). Meanwhile no pale yellow precipitates were formed and no $(UO_2)O_2 \cdot 2H_2O$ was obtained when the SPEC system was operated in N_2 atmosphere (Supplementary Figure 6), suggesting that the DO-mediated $(UO_2)O_2 \cdot 2H_2O$-forming pathway played a vital role in SPEC uranium extraction.

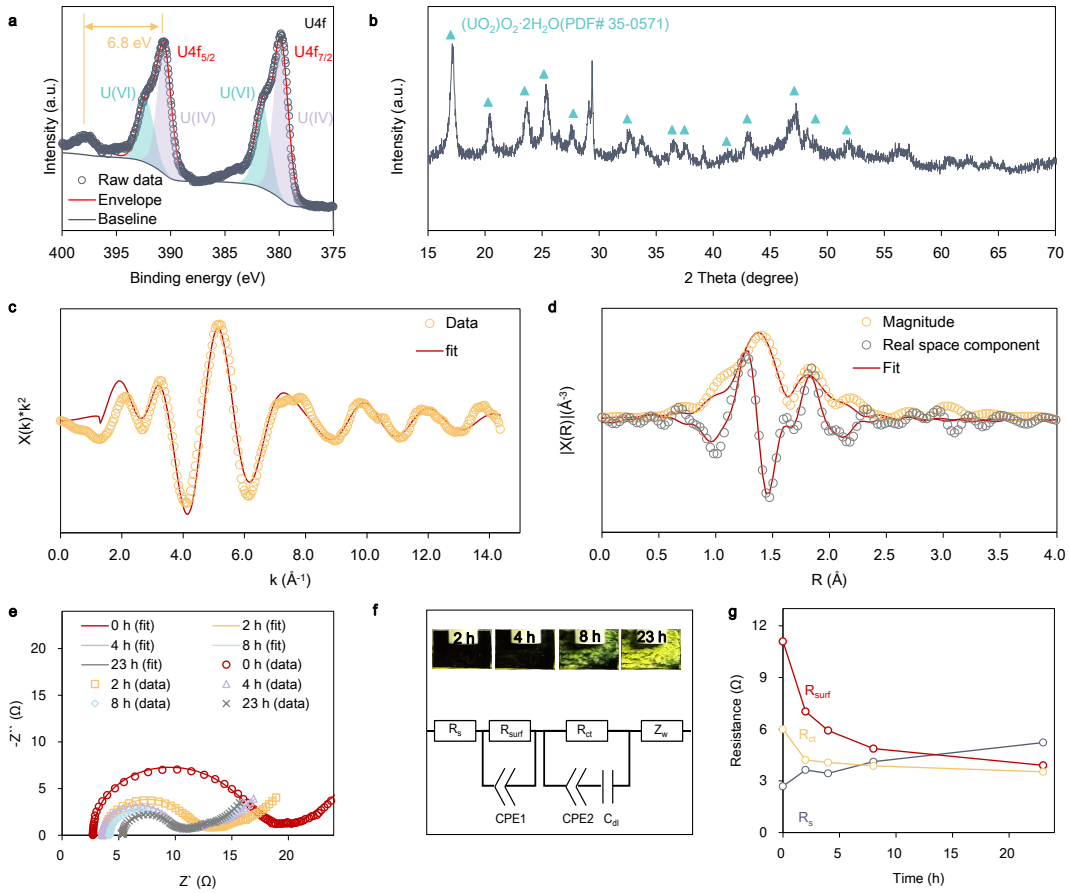

Figure 4. Chemical properties of the extracted uranium. (a) XPS U4f spectrum, (b) XRD pattern, (c) EXFAS k-space analysis and (d) EXFAS R-space analysis of SPEC extracted uranium species; (e) Nyquist plots of the CCF electrode obtained by in-situ EIS tests; (f) The equivalent circuit used for EIS spectra fitting and photographs of the CCF electrode during SPEC uranium extraction; (g) The evolution of different resistance components derived from Nyquist plots shown in (e). Conditions: Simulated wastewater with $[U]_0$ = 100 mg·L^{-1}, unadjusted pH, without external load, effective area of CCF electrode was 2.5 cm^2.

The CCF electrode surface was gradually covered by uranium precipitates (Figure 4f, Supplementary Figure 7, and Supplementary Movie 1), but it did not decelerate the uranium extraction reaction (Supplementary Figure 2d). Previous studies on other electrochemical uranium extraction processes have reported similar findings [3, 13]. These phenomena imply that the uranium precipitates played a vital role in SPEC extraction. Considering that interfacial

electron transfer is a key process for the SPEC uranium extraction, we carried out an in-situ EIS analysis to investigate how the development of the uranium precipitates layer would impact the electron transfer. Figure 4e shows the obtained EIS spectra (Nyquist plots). The obtained EIS spectra consist of a semicircle at the high-middle frequency region, a smaller semicircle at the middle-low frequency region, and an inclined line at the low frequency region, corresponding to the interfacial resistance (R_{suf}), charge transfer resistance (R_{ct}), and Warburg impedance (Z_w), respectively [38, 39, 40, 41]. The fitting results clearly show that both the R_{surf} and the R_{ct} decreased with the development of the uranium precipitates layer during SPEC extraction (Figure 4g and Supplementary Table 2). It evidenced the beneficial role of the uranium precipitates layer: it acts as an important reaction interface that would greatly promote the interfacial electron transfer.

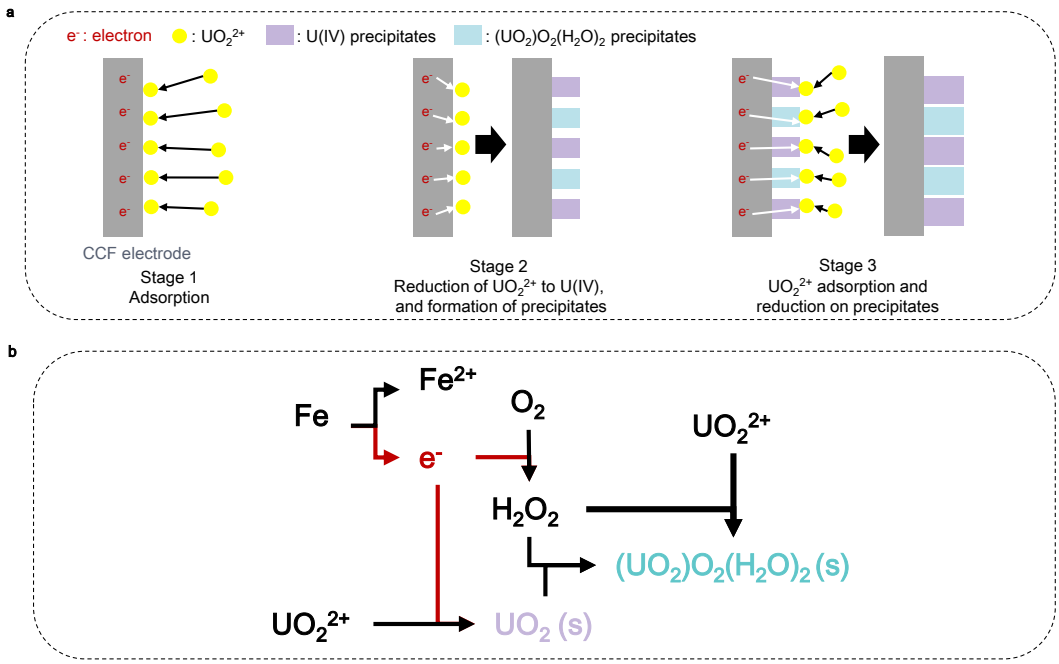

Figure 5. Mechanisms of the SPEC method. (a) The proposed working mechanisms and (b) the schematic representation of the major reaction pathways of the SPEC method.

Based on these results, a probable working mechanism of the SPEC uranium extraction is proposed (Figure 5a). First, aqueous U(VI) species (*i.e.* UO_2^{2+}) are adsorbed onto the surface of the CCF electrode. Second, the adsorbed U(VI) species are reduced to amorphous UO_2 by receiving electrons from the CCF electrode. As shown in Figure 5b, when DO is present, DO

will be reduced to H_2O_2 or $\cdot O_2^-$ species, which will subsequently oxidize part of the UO_2 to $(UO_2)O_2 \cdot 2H_2O$. Both UO_2 and $(UO_2)O_2 \cdot 2H_2O$ are sparingly soluble, which will precipitate on the surface of the CCF electrode, and act as active sites for further uranium extraction. Third, as the electrode surface is covered by the uranium precipitates, the surfaces of precipitates become the dominant reaction venue for U(VI) adsorption and reduction, and the precipitates keep growing.

Recovery of extracted uranium

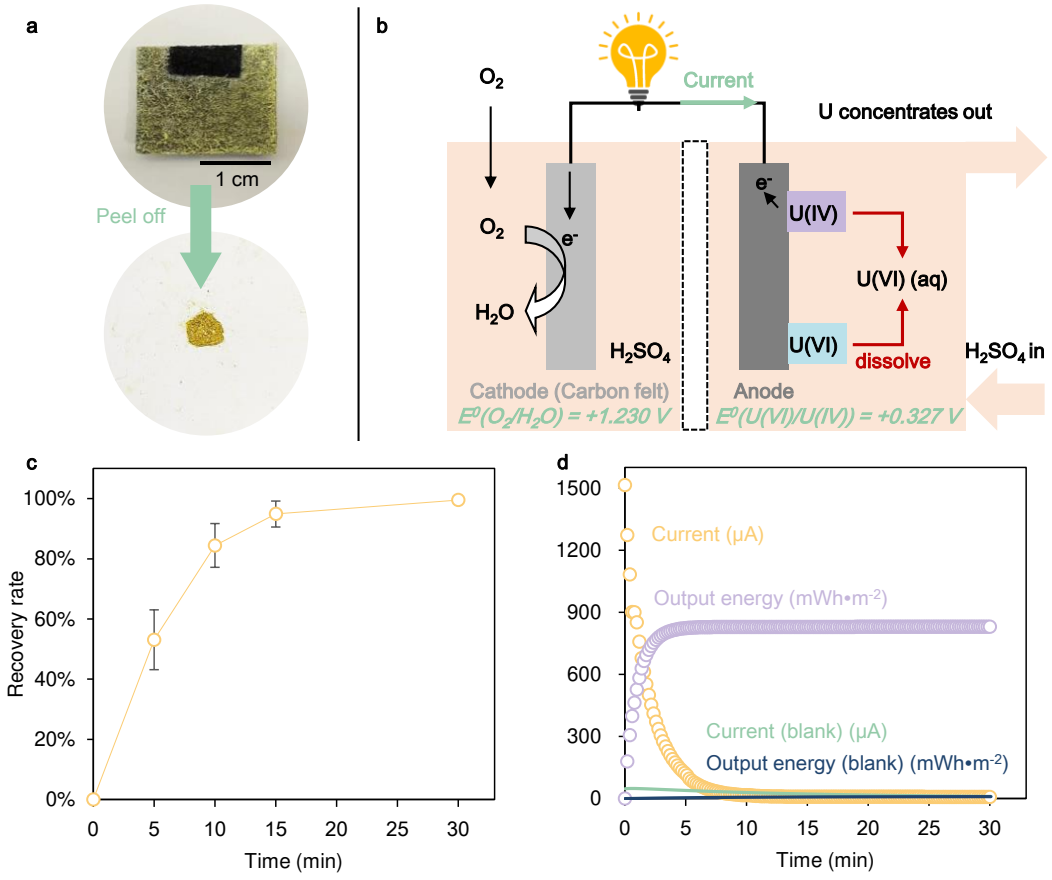

Figure 6. Recovery of extracted uranium. (a) Extracted uranium deposited on the surface of the electrode can be easily peeled-off; (b) The schematic representation of the U(IV)-DO cell concept for the recovery of extracted uranium with simultaneous energy recovery; (c) Uranium recovery using the U(IV)-DO cell; (d) The output current and the accumulated output energy density as a function of time during uranium recovery by the U(IV)-DO cell.

Upon SPEC extraction, the extracted uranium species need to be recovered from the CFF

electrode, for future applications. Because SPEC uranium extraction proceeded via a reduction-precipitation mechanism, the extracted uranium species were fine particles deposited on the electrode. Hence, they can be easily recovered by simply peeling-off from the electrode (Figure 6a). This method is easy-to-operate and is pollution-free. Alternatively, considering that the predominant extraction products are U(IV) species, the extracted uranium can also be recovered with simultaneous electrical energy production by an electrochemical method. The positive E^0 value (+0.327 V vs. SHE) of the U(VI)-to-U(IV) reduction implies that part of the chemical energy from iron oxidation is stored in U(IV) species during SPEC extraction. By coupling the U(IV)-to-U(VI) oxidation with a proper electron acceptor, this chemical energy can be recovered. Meanwhile the rest U(VI) precipitates can be directly dissolved into the recovery solution. Here we chose DO as the electron acceptor, because of its strong oxidation power and its high availability in aqueous solutions exposed to an air atmosphere. Figure 6b shows the schematic representation of the proposed method (more descriptions can be found in the Methods section). The recovery experiment results show that all of the SPEC extracted uranium can be rapidly recovered within a short time frame (Figure 6c), and ~830 $mWh \cdot m^{-2}$ electrical energy was generated.

Validation in real uranium-mine wastewater

SPEC uranium extraction experiments were carried out in real uranium-mine wastewater to validate its feasibility in realistic applications. Photographs of the SPEC modules are shown in Figure 7a. When operated in real-mine wastewater, a single SPEC module could generate an OCV of ~0.820 V and a short-circuit current (SCC) of 0.946 mA (Figure 7b). Similar to the case in simulated wastewater, the electrical energy recovery capacity varies greatly when changing the pH of the H_2SO_4 solution (Supplementary Figure 8). Connecting multiple SPEC modules in series can linearly increase the OCV, while the parallel connection can increase the SCC (Figure 7b), implying the good potential for system scaling up.

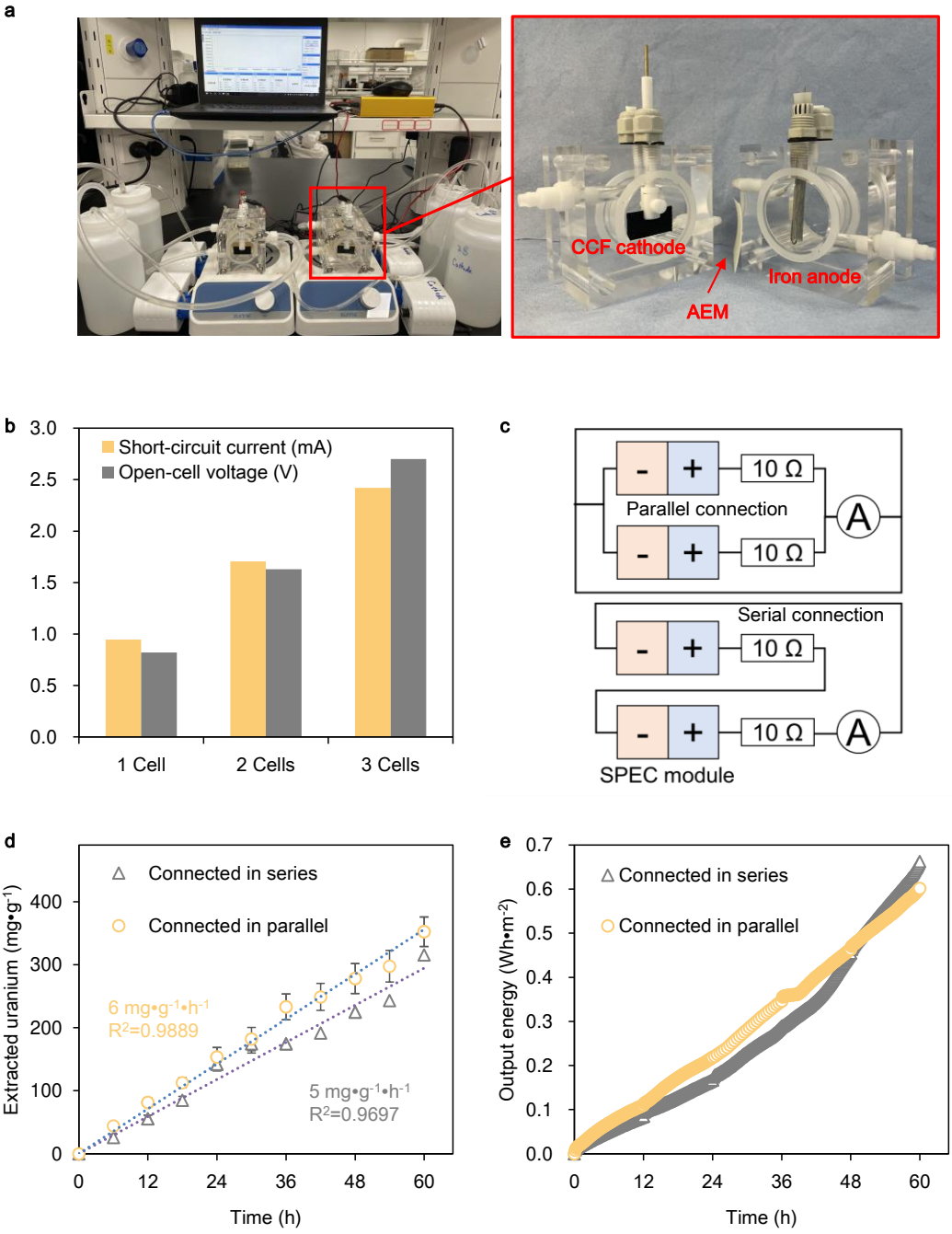

Figure 7. SPEC uranium extraction from real uranium-mine wastewater. (a) Photographs of the SPEC system used for uranium extraction from real wastewater; (b) System OCV (connected in series) and SCC (connected in parallel) versus module numbers; (c) The equivalent circuits of the two-module SPEC system connected in different modes; (d) The long-term uranium extraction performance and (e) electrical energy production performance of the SPEC system.

We then tested the uranium extraction performance using two SPEC modules, operated in different connection modes (equivalent circuit shown in Figure 7c). The results show that the uranium performance of the SPEC system did not vary greatly between different modes (Figure 7d). Upon 60 h continuous operation without changing the CCF cathode, the SPEC system operated in serial connection mode achieved a uranium extraction efficiency of 316 $mg \cdot g^{-1}$, and the extraction efficiency was 352 $mg \cdot g^{-1}$ in parallel mode. The extraction kinetics remained stable throughout the operation (6 $mg \cdot g^{-1} \cdot h^{-1}$ in parallel connection mode and 5 $mg \cdot g^{-1} \cdot h^{-1}$ in serial connection mode). It is noteworthy that, although the uranium-mine wastewater was rather complex with many co-existing metal ions, the uranium was still the predominant metal species in the extraction products as revealed by EDS analysis (Supplementary Figure 9), implying high applicability of the SPEC method in complex water matrices. In addition, during uranium extraction, the SPEC system simultaneously achieved stable electrical energy output (Supplementary Movie 2): upon 60 h operation, 0.65 $Wh \cdot m^{-2}$ and 0.60 $Wh \cdot m^{-2}$ electrical energy in serial connection mode and parallel connection mode was recovered, respectively (Figure 7e). These results prove the uranium extraction and electrical energy generation capabilities of the SPEC method in a realistic application.

Discussion

Uranium extraction from uranium-mine wastewater is of high interest from both the environmental protection and the resource preservation perspectives. In this study, we introduce a spontaneous electrochemical method powered by iron oxidation that can achieve efficient uranium extraction from real mine wastewater, with high stability and relatively good selectivity. The formation of a uranium precipitates layer that provides reactive sites and conducts electron flows is the key to obtaining stable and efficient uranium extraction in electrochemical uranium extraction processes. The mechanistic study reveal a vital role of DO in uranium extraction, which eliminates the need for inert gas atmosphere during operation that was required by previous studies on other electrochemical uranium extraction methods [32]. Moreover, unlike conventional adsorption methods, the extraction products are ready to recover by peeling, without the requirement of desorption operation. In summary, the present study

provides a cost-effective, energy-producing, stable, and easy-to-operate technique for uranium removal and recovery from mine wastewater, contributing to the sustainability of the uranium supply and nuclear power industry.

The iron oxidation reaction is the driving force for the proposed SPEC method. By spatially decoupling the iron-oxidation and the U(VI)-adsorption-reduction reactions, the proposed SPEC method eliminates the drawbacks of conventional nZVI-based methods and adsorption methods. The spatial separation of redox reactions also enables simultaneous electrical energy recovery, eliminating the dependency on electricity input for the electrochemical reduction of U(VI). In addition, part of the chemical energy derived from iron oxidation is stored in the SPEC extracted uranium species, and the stored energy can be subsequently recovered during the recovery of these extraction products. Consequently, unlike current electrochemical extraction technologies that require electricity input, the SPEC uranium extraction process has a net electrical energy production.

Because the SPEC method requires no electricity input, the main operating cost depends on iron consumption. Iron is a very inexpensive resource, and is even available as waste products in many industries [26]. In our bench-scale SPEC uranium extraction experiments with real mine wastewater without process optimization, the operation cost for uranium extraction is calculated to be 3.46~5.99 USD·kgU^{-1} (details in Supplementary Text 1). As a comparison, the current uranium market price is ~152.09 USD·kgU^{-1} in May 2022. Hence, using the proposed SPEC method for uranium extraction from real wastewater is practical and highly cost-effective.

Further optimization and development of the SPEC method are needed to make it fully commercially applicable. For instance, our preliminary investigations found that the flow dynamics and the total area of the CCF working electrode have exerted a noteworthy influence on the uranium extraction kinetics (Supplementary Figure 10). Future studies are encouraged to perform more systematic investigations into the effects of reactor design and operation parameters on SPEC uranium extraction.

Methods

Thermodynamics calculations

Equation 4 shows the general form of the Nernst equation, where $E^0(M^{n+}/M)$ is the potential of a given redox couple under standard conditions, $E(M^{n+}/M)$ is the potential of the redox couple under specific conditions, R is the gas constant, T is the absolute temperature, n is the number of electrons transferred, and F is the Faraday constant. At room temperature (298K), the Nernst equation can be simplified to Equation 5.

$$E(M^{n+}/M) = E^0(M^{n+}/M) + \frac{RT}{nF} ln \frac{[M^{n+}]}{[M]} \quad \textbf{Equation 4}$$

$$E = E^0 + \frac{0.0592}{n} lg \frac{[M^{n+}]}{[M]} \quad \textbf{Equation 5}$$

Uranium extraction experiments

For uranium extraction experiments in simulated wastewater, simulated wastewater was prepared by dissolving $UO_2(NO_3)_2 \cdot 6H_2O$ (Analytical grade, Hubei Qifei Chemical, China) into natural sea water collected from Bohai Bay (China). The sea water used was filtered through a 0.24-μm filter to remove particles and microorganisms. Seawater has high conductivity and contains various co-existing ions, thus it can better mimic the complexity of real wastewaters than ultra-pure water. An H-type two-chambered (300 mL: 300 mL) electrochemical cell was used as the reactor. An iron mesh (20.5 cm^2) was placed in the anode chamber, a CCF electrode (2.5 cm^2, 0.02 g) was placed in the cathode chamber, and an anion exchange membrane (AMI-7001, Membranes International, US) was used to separate the two chambers. 250 mL diluted H_2SO_4 solution with designated pH was filled in the anode chamber, and 250 mL simulated wastewater was filled in the cathode chamber. Unless otherwise noted, the experiments were done in an ambient air atmosphere, and rigorous stirring was applied.

For uranium extraction experiments in real wastewater, uranium-mine wastewater was collected from a granite-type U mine located in western China. The uranium concentration in the real uranium-mine wastewater was measured to be ~7.7 $mg \cdot L^{-1}$ after filtration through a 0.24-μm filter to remove suspended solids and microorganisms. The reactors used for real uranium-mine wastewater experiments were two-chambered (50 mL: 50mL) electrochemical

stack modules (Figure 7a and Supplementary Figure 11). An iron mesh (20.5 cm^2) was placed in the anode chamber, a CCF electrode (4 cm^2, 0.032g) was placed in the cathode chamber, and an anion exchange membrane (AMI-7001, Membranes International, US) was used to separate the two chambers. For each module, 1 L diluted H_2SO_4 solution and 1 L wastewater were stored in storage tanks, respectively. Peristaltic pumps were used to circulate the H_2SO_4 solution and the wastewater through the reactive chambers. The equivalent circuits of the assembled SPEC system using two modules are shown in Figure 7c. During long-term operation, the iron mesh, the H_2SO_4 solution, and the wastewater were changed and refilled every 12 h, without changing the CCF electrode.

During experiments, the current was recorded using an EMK1080 current recorder (Emkia Technology, China). Accumulated output energy density was calculated following the equation below:

$$E_{out} = \int_0^t I^2 R \, dt \, / A_{CCF} \quad \textbf{Equation 6}$$

where E_{out} refers to the accumulated output energy density at time t, I refers to the current, R refers to the external load, A_{CCF} refers to the area of the CCF electrode.

The residual uranium concentration in simulated wastewater was measured by the Arsenazo III spectrophotometric method [13], and the extracted mass of uranium was calculated by comparing the difference between the remaining and the initial uranium concentration in the reaction solution, as instructed by the following equation:

$$q_t = \frac{(C_0 - C_t) \times V}{m} \quad \textbf{Equation 7}$$

where q_t refers to the uranium extraction efficiency at time t, C_0 refers to the initial uranium concentration in the reaction solution, C_t refers to the uranium concentration in the reaction solution at time t, m refers to the mass of the CCF electrode, V refers to the volume of the reaction solution.

Recovery of extracted uranium

For extracted uranium recovery experiments, an H-type two-chambered (300 mL: 300 mL) electrochemical cell was used as the reactor. The CCF electrode covered by the known amount

of SPEC extracted uranium (2.5 cm^2) was placed in the anode chamber, a carbon felt electrode (4.5 cm^2) was placed in the cathode chamber, and an anion exchange membrane (AMI-7001, Membranes International, US) was used to separate the two chambers. 250 mL of air-saturated 0.1M H_2SO_4 solution was filled in both chambers. A 100 Ω resistor was connected between the two electrodes. Blank control experiments were also performed, by replacing the uranium-covered CCF electrode with a fresh CCF electrode.

During experiments, the current was recorded using an EMK1080 current recorder (Emkia Technology, China). The uranium concentration in anolyte was measured by the Arsenazo III spectrophotometric method, and the recovery rate was calculated by comparing the difference between the mass of recovered uranium in anolyte and the initial uranium mass on the CCF electrode, as instructed by the following equation:

$$R_t = \frac{C_t \times V_a}{M_{CCF}} \times 100\% \quad \textbf{Equation 8}$$

where R_t refers to the uranium recovery rate at time t, C_t refers to the uranium concentration in the reaction solution in the anode chamber at time t, M_{CCF} refers to the initial uranium mass on CCF electrode, V_a refers to the volume of the reaction solution in the anode chamber.

Characterizations

Scanning electron microscopy (SEM) and energy dispersive spectroscopy (EDS) were conducted using a Tescan Mira 4 FE-SEM equipped with an Xplore 30 EDS system. X-ray photoelectron spectroscopy (XPS) characterization was carried out using a Thermo K-Alpha+ XPS with an Al (Kα) source. X-ray diffraction (XRD) characterization was carried out using a Rigaku D-Max 2500PC XRD with Cu Kα radiation. For EXAFS analysis, the CCF electrode deposited with SPEC uranium extraction products was analyzed at the BL14W1 beamline of the Shanghai Synchrotron Radiation Facility at room temperature with a Zr foil serving as the reference for calibration. The obtained spectrum was processed by using the ATHENA and ARTEMIS programs [42]. The crystal structure of metastudtite was archived from Weck et al.[43], and used as the starting model for EXAFS fitting, following the procedures described by Walshe et al.[44]. Linear sweep voltammetry (LSV) and in-situ electrochemical Impedance Spectroscopy

(EIS) characterizations of the CCF electrode were carried out using a CHI660E electrochemical workstation.

Acknowledgements

This work was supported by the National Natural Science Foundation of China (No. 42077352), and the Fundamental Research Funds for the Central Universities (No. 31020200QD024, No. 3102019JC007, G2021KY0601).

Author contributions

Conceptualization, Y.Y., F.C., and J.J.; Formal Analysis, Y.Y. and J.J.; Funding Acquisition, Y.Y., F.C., and Y.W.; Investigation, J.J., W.H., X.T., Z.Q., Y.C., C.L, Y.F., and S.M.; Methodology, Y.Y., F.C., and J.J.; Project Administration, Y.Y., F.C., and Y.W.; Resources, Y.Y., F.C., S.M., and Y.W.; Supervision, Y.Y., F.C., and Y.W.; Validation, Y.Y., F.C., and Y.W.; Visualization, Y.Y.; Writing – Original Draft, Y.Y.; Writing – Review & Editing, F.C., Y.W. and Y.F..

Declaration of interests

The authors declare no competing financial interests.

References

1. Rhodes R. More nuclear power can speed CO_2 cuts. *Nature* **548**, 281 (2017).

2. NEA, IAEA. *Uranium 2020* (2021).

3. Liu C*, et al.* A half-wave rectified alternating current electrochemical method for uranium extraction from seawater. *Nature Energy* **2**, 17007 (2017).

4. Abney CW, Mayes RT, Saito T, Dai S. Materials for the Recovery of Uranium from Seawater. *Chemical Reviews* **117**, 13935-14013 (2017).

5. Tsouris C. Uranium extraction: Fuel from seawater. *Nature Energy* **2**, 17022 (2017).

6. Zheng M, Ji H, Duan J, Dang C, Chen X, Liu W. Efficient adsorption of europium (III) and uranium (VI) by titanate nanorings: Insights into radioactive metal species. *Environmental Science and Ecotechnology* **2**, 100031 (2020).

7. Tsarev S, Collins RN, Fahy A, Waite TD. Reduced Uranium Phases Produced from Anaerobic Reaction with Nanoscale Zerovalent Iron. *Environmental Science & Technology* **50**, 2595-2601 (2016).

8. Yuan Y*, et al.* Selective extraction of uranium from seawater with biofouling-resistant polymeric peptide. *Nature Sustainability* **4**, 708-714 (2021).

9. Yuan Y*, et al.* Ultrafast and Highly Selective Uranium Extraction from Seawater by Hydrogel-like Spidroin-based Protein Fiber. *Angewandte Chemie International Edition* **58**, 11785-11790 (2019).

10. Yang L*, et al.* Bioinspired hierarchical porous membrane for efficient uranium extraction from seawater. *Nature Sustainability* **5**, 71-80 (2022).

11. Cui W-R*, et al.* Regenerable and stable sp2 carbon-conjugated covalent organic frameworks for selective detection and extraction of uranium. *Nature Communications* **11**, 436 (2020).

12. Yuan Y, Feng S, Feng L, Yu Q, Liu T, Wang N. A Bio-inspired Nano-pocket Spatial Structure for Targeting Uranyl Capture. *Angewandte Chemie International Edition* **59**, 4262-4268 (2020).

13. Yang H*, et al.* Functionalized Iron–Nitrogen–Carbon Electrocatalyst Provides a Reversible Electron Transfer Platform for Efficient Uranium Extraction from Seawater. *Advanced Materials* **33**, 2106621 (2021).

14. Wang Z*, et al.* Constructing an Ion Pathway for Uranium Extraction from Seawater. *Chem* **6**, 1683-1691 (2020).

15. Chi F, Zhang S, Wen J, Xiong J, Hu S. Highly Efficient Recovery of Uranium from Seawater Using an Electrochemical Approach. *Industrial & Engineering Chemistry Research* **57**, 8078-8084 (2018).

16. Gu B, Liang L, Dickey MJ, Yin X, Dai S. Reductive Precipitation of Uranium(VI) by Zero-Valent Iron. *Environmental Science & Technology* **32**, 3366-3373 (1998).

17. Fiedor JN, Bostick WD, Jarabek RJ, Farrell J. Understanding the Mechanism of

Uranium Removal from Groundwater by Zero-Valent Iron Using X-ray Photoelectron Spectroscopy. *Environmental Science & Technology* **32**, 1466-1473 (1998).

18. Zhao X, Liu W, Cai Z, Han B, Qian T, Zhao D. An overview of preparation and applications of stabilized zero-valent iron nanoparticles for soil and groundwater remediation. *Water Research* **100**, 245-266 (2016).

19. Ruan Y*, et al.* Phosphate enhanced uranium stable immobilization on biochar supported nano zero valent iron. *Journal of Hazardous Materials* **424**, 127119 (2022).

20. Zhang X*, et al.* Controllable shell corrosion of coated nanoscale zero valent iron induces long-term potentiation of its reactivity for uranium removal. *Separation and Purification Technology* **287**, 120550 (2022).

21. Ling L, Zhang W-x. Enrichment and Encapsulation of Uranium with Iron Nanoparticle. *Journal of the American Chemical Society* **137**, 2788-2791 (2015).

22. Tsarev S, Collins RN, Ilton ES, Fahy A, Waite TD. The short-term reduction of uranium by nanoscale zero-valent iron (nZVI): role of oxide shell, reduction mechanism and the formation of U(v)-carbonate phases. *Environmental Science: Nano* **4**, 1304-1313 (2017).

23. Bae S, Collins RN, Waite TD, Hanna K. Advances in Surface Passivation of Nanoscale Zerovalent Iron: A Critical Review. *Environmental Science & Technology* **52**, 12010-12025 (2018).

24. Mortazavian S, An H, Chun D, Moon J. Activated carbon impregnated by zero-valent iron nanoparticles (AC/nZVI) optimized for simultaneous adsorption and reduction of aqueous hexavalent chromium: Material characterizations and kinetic studies. *Chemical Engineering Journal* **353**, 781-795 (2018).

25. Guan X*, et al.* The limitations of applying zero-valent iron technology in contaminants sequestration and the corresponding countermeasures: The development in zero-valent iron technology in the last two decades (1994–2014). *Water Research* **75**, 224-248 (2015).

26. Sun M*, et al.* Electrochemical-Osmotic Process for Simultaneous Recovery of Electric Energy, Water, and Metals from Wastewater. *Environmental Science & Technology* **54**, 8430-8442 (2020).

27. Li P*, et al.* Uranium elimination and recovery from wastewater with ligand chelation-enhanced electrocoagulation. *Chemical Engineering Journal* **393**, 124819 (2020).

28. Yang P, Li S, Liu C, Shen C, Liu X. Water-endurable intercalated graphene oxide adsorbent with highly efficient uranium capture from acidic wastewater. *Separation and Purification Technology* **263**, 118364 (2021).

29. Cheng Y*, et al.* Polyamine and amidoxime groups modified bifunctional polyacrylonitrile-based ion exchange fibers for highly efficient extraction of U(VI) from real uranium mine water. *Chemical Engineering Journal* **367**, 198-207 (2019).

30. Li J*, et al.* Removal of uranium from uranium plant wastewater using zero-valent iron in an ultrasonic field. *Nuclear Engineering and Technology* **48**, 744-750 (2016).

31. Wang J*, et al.* Surface water contamination by uranium mining/milling activities in

Northern Guangdong Province, China. *CLEAN – Soil, Air, Water* **40**, 1357-1363 (2012).

32. Liu T*, et al.* Removal and recovery of uranium from groundwater using direct electrochemical reduction method: Performance and implications. *Environmental Science & Technology* **53**, 14612-14619 (2019).

33. Yuan K, Renock D, Ewing RC, Becker U. Uranium reduction on magnetite: Probing for pentavalent uranium using electrochemical methods. *Geochimica et Cosmochimica Acta* **156**, 194-206 (2015).

34. Yuan K, Ilton ES, Antonio MR, Li Z, Cook PJ, Becker U. Electrochemical and Spectroscopic Evidence on the One-Electron Reduction of U(VI) to U(V) on Magnetite. *Environmental Science & Technology* **49**, 6206-6213 (2015).

35. Corbel C, Sattonnay G, Guilbert S, Garrido F, Barthe MF, Jegou C. Addition versus radiolytic production effects of hydrogen peroxide on aqueous corrosion of UO2. *Journal of Nuclear Materials* **348**, 1-17 (2006).

36. Guo X, Ushakov SV, Labs S, Curtius H, Bosbach D, Navrotsky A. Energetics of metastudtite and implications for nuclear waste alteration. *Proceedings of the National Academy of Sciences* **111**, 17737-17742 (2014).

37. Kubatko K-AH, Helean KB, Navrotsky A, Burns PC. Stability of Peroxide-Containing Uranyl Minerals. *Science* **302**, 1191-1193 (2003).

38. Li X*, et al.* High valence Mo-doped Na3V2(PO4)3/C as a high rate and stable cycle-life cathode for sodium battery. *Journal of Materials Chemistry A* **6**, 1390-1396 (2018).

39. Li Q*, et al.* Silica Restricting the Sulfur Volatilization of Nickel Sulfide for High-Performance Lithium-Ion Batteries. *Advanced Energy Materials* **9**, 1901153 (2019).

40. Zahiri B*, et al.* Revealing the role of the cathode–electrolyte interface on solid-state batteries. *Nature Materials* **20**, 1392-1400 (2021).

41. Boyle DT*, et al.* Corrosion of lithium metal anodes during calendar ageing and its microscopic origins. *Nature Energy* **6**, 487-494 (2021).

42. Ravel B, Newville M. ATHENA, ARTEMIS, HEPHAESTUS: data analysis for X-ray absorption spectroscopy using IFEFFIT. *Journal of Synchrotron Radiation* **12**, 537-541 (2005).

43. Weck PF, Kim E, Jové-Colón CF, Sassani DC. Structures of uranyl peroxide hydrates: a first-principles study of studtite and metastudtite. *Dalton Transactions* **41**, 9748-9752 (2012).

44. Walshe A, Prüßmann T, Vitova T, Baker RJ. An EXAFS and HR-XANES study of the uranyl peroxides [UO2(η2-O2)(H2O)2]·nH2O (n = 0, 2) and uranyl (oxy)hydroxide [(UO2)4O(OH)6]·6H2O. *Dalton Transactions* **43**, 4400-4407 (2014).

Supplementary Files

This is a list of supplementary files associated with this preprint. Click to download.

- SupplementaryInformation.pdf
- Supplementarymovie1.mp4
- Supplementarymovie2.mp4